ANFIS and Takagi-Sugeno interval observers for fault diagnosis in bioprocess system

Esvan-Jesús Pérez-Pérez[b], José-Armando Fragoso-Mandujano[a], Julio-Alberto Guzmán-Rabasa[c], Yair González-Baldizón[a], Sheyla-Karina Flores-Guirao[a]

[a] *Tecnológico Nacional de México, I.T. Tuxtla Gutiérrez, Carretera Panam. km 1080, CP 29050, Tuxtla Gutiérrez, Chiapas, México.*
[b] *Universitat Politècnica de Catalunya, Institut de Robòtica i Informàtica Industrial, CSIC-UPC. Parc Tecnològic de Barcelona. C Llorens i Artigas 4-6, 08028, Barcelona, Spain.*
[c] *Tecnológico Nacional de México, I.T. Hermosillo, Av. Tecnológico y Periférico Poniente, S/N, 83170, Hermosillo, México.*

Abstract

This paper develops a data-driven approach for incipient fault diagnosis based on ANFIS and Takagi-Sugeno (TS) interval observers. First, the nonlinear bioreactor system is identified using an adaptive neuro-fuzzy inference system (ANFIS), which results in a set of polytopic TS models derived from measurement data. Second, a bank of TS interval observers is deployed to detect sensor and process faults using adaptive thresholds. Unlike other works that require training fault data, only fault-free data is considered for ANFIS learning in this work. Fault insolation is based on residual generation and evaluated on a fault signal matrix (FSM). Parametric uncertainty and measurement noise are considered to guarantee the method's robustness. The effectiveness of the proposed method is tested on a well-known bioreactor Continuous stirred tank reactor system (CSTR) reference simulator.

Keywords: Takagi-Sugeno observers, fault diagnosis, ANFIS, bioreactor

*Corresponding author
Email address: jose.fm@tuxtla.tecnm.mx (José-Armando Fragoso-Mandujano)

1. Introduction

Bioreactors, at their core, are vessels in which biological processes are carried out under controlled conditions. They are fundamental tools in biotechnology, used for cultivating cells or microorganisms to produce a wide range of products, from pharmaceuticals to biofuels [1]. Bioreactors are designed to provide the optimal environment for achieving desired biochemical transformations, with precise control over factors such as temperature, pH, oxygen supply, and substrate concentration [2].

Despite their critical role, bioreactors are systems subject to various potential risks. One of the primary concerns is the occurrence of operational faults, which can arise due to equipment faults, process deviations, or biological factors such as contamination or unexpected cellular behavior [3]. These faults can lead to significant consequences, including reduced product performance [4], compromised product quality [5], and, in some cases, complete process fault [6]. Bioprocess faults can have serious consequences, from losing valuable products to potentially dangerous situations. In high-risk industries, such as pharmaceuticals, these faults can lead to substantial financial losses and delays in the availability of products [7].

Motivated by these risks, developing robust fault detection and monitoring systems is crucial. Such systems must identify and isolate faults quickly and adapt to biological processes' complex and dynamic nature [8]. This has motivated the development of new monitoring and control schemes in bioreactors, where advanced technologies such as machine learning and artificial intelligence are used [9].

Implementing fault detection and mitigation strategies is essential to guarantee the stability and safety of these production processes [10]. Therefore, new fault detection methods are necessary for the successful and sustainable operation of chemical systems and bioprocesses in industrial and research environments,[11].

Various strategies have addressed faults in CSTR reactors; the essential methodologies over recent years are presented below, in [12] investigated the detection and diagnosis of faults in a CSTR reactor using artificial neural networks using online approaches. Similarly, [13] presented a comprehensive fault detection, diagnosis, and fault-tolerant control strategy, highlighting the importance of proportional-integral-derivative (PID) state feedback in FTC against sensor faults. In that same sense, [14] developed a fault-tolerant active control scheme for nonlinear processes by integrating a nonlinear version of the method based on the generalized probability index applied to CSTR systems. For their part, [15] presented an algorithm for detecting and identifying faults in nonlinear systems, combining the extended Kalman filter and neuro-fuzzy networks applied specifically to CSTR.

A scheme for sensor fault detection in CSTR reactor processes was presented in [16], using an unknown input observer (UIO), exploring the concept of cross-domain fault diagnosis. In [17] presented a comprehensive design that includes a concentration estimator and a fault-tolerant control strategy to compensate for failures in a CSTR actuator. This study also compared nonlinear, linear, and quasilinear models with variable parameters (qLPV) in CSTR systems. For example, [18] proposed a fault-tolerant control strategy that monitors the distance of the system state from the boundary of the dynamic safe set and estimates the size of the fault.

Various works based on models for fault detection have been reported. For example, in [19], the problem of designing functional observers to diagnose failures in nonlinear systems in the presence of noise was addressed; the effect of sensor noise on fault detection residuals was analytically studied. A robust interval observer was designed to estimate the state and measured output of a dark biohydrogen fermenter. The concentrations of glucose and biomass were estimated, reducing the influence of uncertainty, and faults were detected in sensors [20]. In [21], an estimation of faults in sensors and actuators was proposed with a control system in a wastewater treatment plant (WWTP), using the system with a discrete TS fuzzy model to identify the system; fault detection was performed using dual TS observers. Also, in [22], a fault detection scheme for sensors and actuators in a WWTP was presented based on low-order TS models and a generalized sliding mode observer. In [23], a UIO-type observer was designed to detect and isolate faults in two bioreactors. The system has uncertain nonlinear time delays; the method is robust to production disturbances.

In this context, ANFIS techniques emerge as novel approaches for studying faults in CSTR reactors, offering an advanced paradigm that combines the adaptability of fuzzy systems with the learning capacity of neural networks, thus providing a unique and practical perspective for analyzing and detecting faults in these systems. The work of [24] explored fault-tolerant control using a dedicated observer based on an adaptive neuro-fuzzy inference system (ANFIS), complemented by state feedback control supported by a linear quadratic regulator (LQR) in situations of an abrupt sensor fault. However, [25] used the subtractive clustering technique to determine the ANFIS structure; this approach was highlighted when implementing a soft sensor in a chemical plant and reaching it with an ANFIS-based soft sensor that is based on a quadratic cost function. Also, the proposal in [26] focused on a learning approach named "Extreme-ANFIS". This method was used to adjust the assumptions and parameters associated with the Takagi-Sugeno Fuzzy Inference System (TS-FIS) because it is fast and straightforward.

This work proposes a hybrid approach to diagnose incipient faults of bioprocess systems based on data-driven neuro-fuzzy techniques and Takagi-Sugeno interval observers. It is highlighted that the identification of the dynamic system of the bioreactor is based on ANFIS learning, which structures a set of convex Takagi-Sugeno models. ANFIS is trained only with fault-free data. Then, fault detection is carried out based on the residual generation obtained by the interval observers, affected by measurement uncertainty and noise. Different fault scenarios are considered and evaluated with a fault signal matrix. The main contributions of this work can be listed as follows:

- A hybrid approach combining ANFIS neuro-fuzzy systems and TS interval observers for detecting and isolating incipient faults.
- Utilization of fault-free system measurements for model identification in

ANFIS, avoiding the need for various types of fault data typically required in other methodologies.

- Development of interval observers based on TS models that provide robust fault detection against parametric uncertainty and measurement noise.
- A practical, data-driven scheme that eliminates the necessity for complex, calibrated models, leveraging the adaptability of ANFIS and the precision of interval observers under adaptive thresholds.

This document is organized as follows: Section 2 presents the case study, fault scenarios, and data preparation. Section 3 describes the fault diagnosis methodology, the structure of the ANFIS, and the design of the interval observers; then Section 4 presents the results; finally, Section 5 presents the conclusions.

2. Model of bioreactor CSTR system

Below is a generic model based on fundamental principles for a CSTR bioreactor system that operates continuously in a second-order exothermic reaction, validated in [27] and [28], where species A becomes species B. The equations (1–3) are material and energy balances for a chemical process.

$$\frac{dC}{dt} = \frac{Q}{V}\left(C_i - C\right) - akC + \nu_1 \tag{1}$$

$$\frac{dT}{dt} = \frac{Q}{V}\left(T_i - T\right) - a\frac{(\Delta H_r)kC}{\rho C_p} - b\frac{UA}{\rho C_p V}\left(T - T_c\right) + \nu_2 \tag{2}$$

$$\frac{dT_c}{dt} = \frac{Q_c}{V_c}\left(T_{ci} - T_c\right) + b\frac{UA}{\rho_c C_{pc} V_c}\left(T - T_c\right) + \nu_3 \tag{3}$$

where the bioreactor process variables encompass C_i, the molar concentration of the inlet reactant, and the concentration C of output product . Both are pivotal for the reaction's progress and are measured in moles per liter. The reactor's operational temperature is given by T, while T_c indicates the temperature of the cooling or heating jacket, both vital for managing the reaction rate and measured in Kelvin. The coolant flow-rate Q_c, measured in liters per minute, is essential for maintaining the reactor temperature. The variables C_i, T_i, and T_{ci} denote the entering reactant concentration, temperature, and coolant temperature, respectively, which are critical for establishing the starting conditions of the reaction process. The k is an Arrhenius-type rate constant, $\mathbf{u} = \begin{bmatrix} C_i & T_i & T_{ci} \end{bmatrix}^T$ and $\mathbf{y} = \begin{bmatrix} C & T & T_c & Q_c \end{bmatrix}^T$ are the inputs and outputs respectively, and ν_i represents the process noise. The values of constant process parameters are listed in Table 1.

Table 1: Constant values in the CSTR model

Parameter	Description	Value	Units
k_0	Pre-exponential factor to k	7.2×10^{10}	min^{-1}
ρ, ρ_c	Fluid density	Q	g/L
C_p, C_{pc}	Fluid heat capacity	1	cal/g/K
ΔH_r	Heat of reaction	-2×10^5	cal/mol
UA	Heat transfer coefficient	7×10^5	cal/min/K
E/R	Activation energy	1×10^4	K
V	Trank volume	150	L
V_c	Jacket volume	10	L
Q	Inlet flow-rate	100	L/min

The CSTR schematic in Figure 1 illustrates the configuration, highlighting measurement points and the implemented control strategy. Specifically, the reactor temperature (T) is regulated by adjusting the coolant flow-rate (Q_c). For added realism, the controller parameters ($K_c = 1.0$ and $\tau_I = 0.2$) are configured to saturate below 10 L/min and above 200 L/min. Intentionally introducing saturation is essential for simulating scenarios where a developing fault escalates to a point where control mechanisms cannot effectively manage it. In the model, both parameters a and b are initially set to 1.00 during normal operation. The simulation can replicate catalyst decay and heat transfer fouling by gradually reducing these values to zero. Additionally, various faults in the system include sensor drifts affecting each of the seven measured variables. Further information on these potential fault scenarios is provided in Table 2.

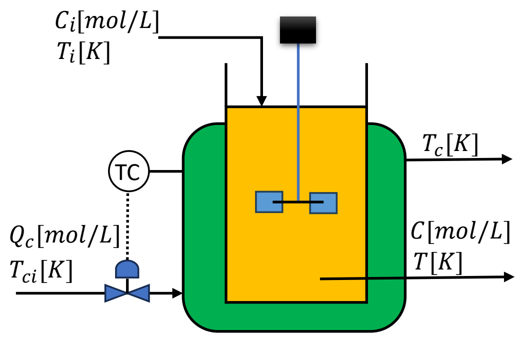

Figure 1: Scheme representing a closed-loop CSTR.

Table 2: Fault Cases in CSTR

Fault ID	Description	Value of δ	Type
1	$a = a_0 \exp(-\delta t)$	0.0005	Multiplicative
2	$b = b_0 \exp(-\delta t)$	0.001	Multiplicative
3	Simultaneous Faults 1 and 2	-	Multiplicative
4	$C = C_0 + \delta t$	0.001	Additive
5	$T = T_0 + \delta t$	0.05	Additive
6	$T_{ci} = T_{c,0} + \delta t$	0.05	Additive
7	$Q_c = Q_{c,0} + \delta t$	-0.1	Additive

2.1. Preparation of data for ANFIS training

135 Preparing CSTR system data involves conducting simulations over a duration of 1200 minutes at a sampling frequency of 4 samples per minute. These simulations are carried out under fault-free conditions. System inputs are generated using a random seed and are subject to measurement noise during the simulations. Since the proposed scheme is data-driven, data is collected from

Table 3: Output variables to be estimated in regressive form

Output y_i	Regressive form
$\hat{C}(k)$	$(C(k), C(k-1), C(k-2), C_i(k), T_i(k), T_{ci}(k))$
$\hat{T}(k)$	$(T(k), T(k-1), T(k-2), C_i(k), T_i(k), T_{ci}(k))$
$\hat{T}_c(k)$	$(T_c(k), T_c(k-1), T_c(k-2), C_i(k), T_i(k), T_{ci}(k))$
$\hat{Q}_c(k)$	$(Q_c(k), Q_c(k-1), Q_c(k-2), C_i(k), T_i(k), T_{ci}(k))$

both input and output sensors. A crucial consideration in data preparation is addressing the inherent nonlinearity of the CSTR system. To effectively capture this nonlinearity, variables are estimated regressively, incorporating information from two previous instances k. This approach enhances the modeling of complex and nonlinear relationships in the system's behavior. The estimated output variables related to input are structured in the regressive form, as detailed in Table 3.

These regressive expressions will serve as inputs for the ANFIS networks, and through learning, they can identify the estimated variables and obtain Takagi-Sugeno models to design the interval observers.

3. Hybrid fault diagnosis scheme for the CSTR system

This section presents a hybrid method for fault diagnosis in CSTR bioreactors, utilizing exclusively available measurement data during the operational process, as shown in Figure 2. This approach centers around applying Adaptive Neuro-Fuzzy Inference Systems (ANFIS) to identify the inherent nonlinear dynamic of the bioreactor, with the training process utilizing fault-free operational data for capturing system dynamics under normal conditions. Building on the learning acquired from ANFIS, generated sets of Takagi-Sugeno systems provide a more accurate representation of the bioreactor's behavior under adaptative operational conditions. To enhance fault detection, design interval observers with adaptable thresholds, dynamically adjusting to variations in system conditions and intervening in the early detection of anomalies, thereby improving process reliability and safety. Finally, fault isolation is addressed through an analysis of the fault incidence matrix, offering an efficient strategy for identifying the location and nature of potential faults within the CSTR bioreactor.

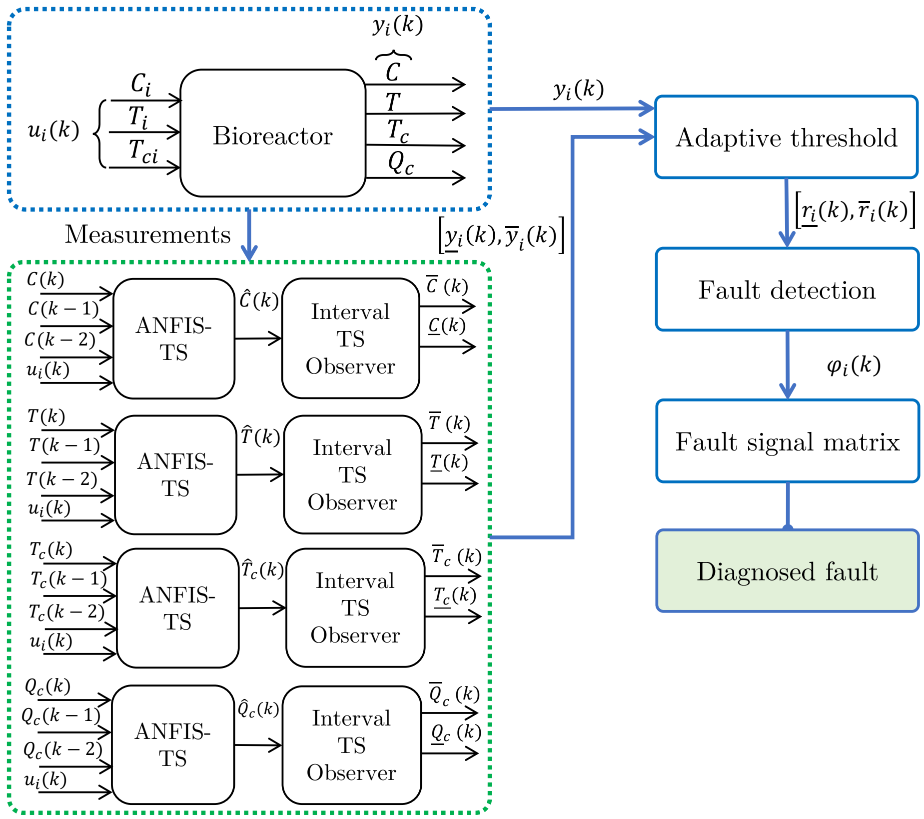

Figure 2: Hybrid scheme for fault diagnosis in CSTR.

3.1. Obtaining Takagi Sugeno systems from ANFIS learning

Neuro-fuzzy approaches, integrating the advantages of artificial neural networks and fuzzy inference systems, have been instrumental in identifying nonlinear behaviors [29]. The ANFIS generates a weighted sum of linear models using a multilayer feedforward network consisting of antecedent and consequent parts. Hybrid training algorithms are then employed to ascertain the neuro-fuzzy parameters corresponding to each part of the network. As illustrated in Figure 3, the ANFIS builds a Takagi-Suigeno model to approximate the variables outputs of bioreactor $\mathbf{y}$. For example, the input vector θ incorporates variable estimate C, encompassing values such as $C(k)$, $C(k-1)$, $C(k-2)$, $C_i(k)$, $T_i(k)$, and $T_{ci}(k)$. ANFIS captures the nonlinear behavior and is expressed as polytopic Takagi-Sugeno models. The learning stage utilizes fault-free sensor data, structured to include the input data for ANFIS. The ANFIS model approximates

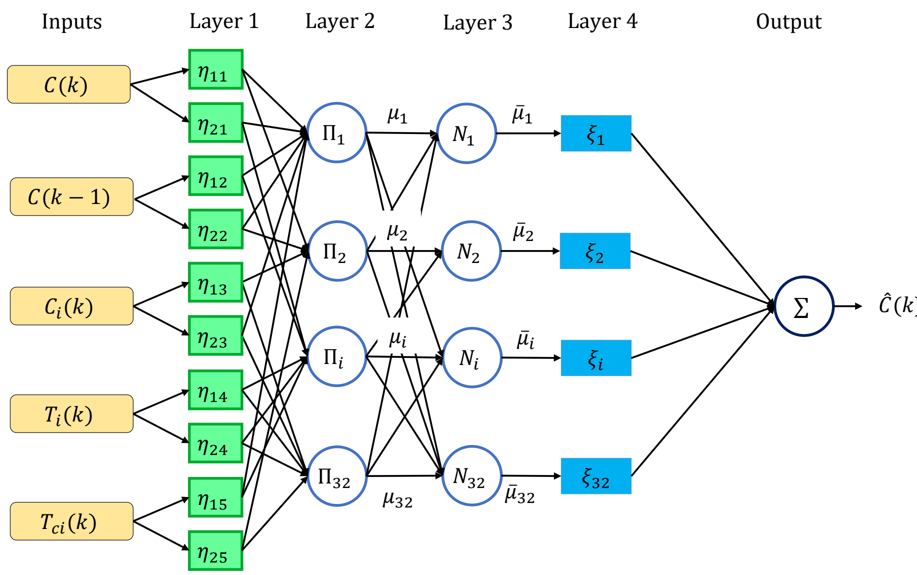

Figure 3: ANFIS architecture to identify the C variable.

the nonlinear behavior of the bioreactor and is represented through polytopic Takagi-Sugeno models. The datasets utilized during the learning stage consist of fault-free sensor data. The input data for ANFIS are constructed for each output $\mathbf{y}$ and are organized as follows:

$$\theta = \begin{bmatrix} C(k) & C(k-1) & C(k-2) & C_i(k) & T_i(k) & T_{ci}(k) \end{bmatrix}^T . \quad (4)$$

Layer 1: Known as fuzzification or the antecedent/premise layer, this layer employs Generalized Bell-Shaped membership functions (MF) for fuzzification. Each Bell-Shaped function, denoted as $\eta(\cdot)$, is characterized by three neuro-fuzzy parameters (a_{mo}, b_{mo}, c_{mo}). The function is defined as $\eta_{mo}(\theta_o) = \frac{1}{1+\frac{\theta_o - c_{mo}}{a_{mo}}^{2b_{mo}}}$, where θ represents the vector of ANFIS input variables (referred to as scheduling parameters), N_{MF} represents the number of MF per scheduling parameter, and the parameters are adjusted during training epochs.

Layer 2: This layer generates rules utilizing the previously defined Bell-Shaped functions. Each of the $N_v = (N_{MF})^{N_\theta} = 64$ nodes is a fixed node that multiplies incoming signals and sends the product. The computation is expressed as $\mu_i(\theta) = \prod_{o=1}^{N_\theta} \eta_{mo}(\theta_o)$, where each scheduling parameter θ_o is estimated and varies within a defined interval $\theta_o \in \left[\underline{\theta_o}, \overline{\theta_o}\right] \subset \mathbb{R}$.

Layer 3: This normalization layer computes the weighted values associated with each rule as $\bar{\mu}_i(\theta) = \frac{\mu_i(\theta)}{\sum_{i=1}^{N_v} \mu i(\theta)}$.

Layer 4: Referred to as defuzzification or the consequent layer, this layer employs the fuzzy if-then rules of Takagi and Sugeno [29]. The rules are expressed as $\mathcal{R}_i : IF \quad \theta_1 \quad is \quad \eta_{m1} \quad AND, \ldots, AND \quad \theta_{N_\theta} \quad is$ $\eta_{mN_\theta} \quad THEN \quad \bar{\mu}_i \xi_i = \bar{\mu}_i(\theta_i p_i + h_i), \quad \forall i = 1, \ldots, N_v$.

Output: This layer determines the overall output by summing all incoming signals from the defuzzification layer, i.e., $\sum_{i=1}^{N_v} \bar{\mu}_i \xi_i$.

After the completion of ANFIS training and the computation of normalized weights along with consequent parameters, the subsequent step involves the construction of the polytopic Takagi-Sugeno representation. For this illustration, we consider the case of C, which is formulated as follows:

$$\hat{C}(k) = \sum_{i=1}^{N_v} \bar{\mu}_i(\theta(k)) \Big(p_{1i} C(k) + p_{2i} C(k-1) p_{3i} C(k-2) + p_{4i} C_i(k) + p_{5i} T_i(k) + p_{6i} T_{ci}(k) + h_i \Big). \tag{5}$$

Terms in (5) can be rearranged as:

$$\hat{C}(k) = \sum_{i=1}^{N_v} \begin{bmatrix} \bar{\mu}_i^1(\theta(k)) \\ \bar{\mu}_i^2(\theta(k)) \\ \bar{\mu}_i^3(\theta(k)) \end{bmatrix} \left(\overbrace{\begin{bmatrix} p_{1i}^1 & p_{2i}^1 & p_{3i}^1 \\ p_{1i}^2 & p_{2i}^2 & p_{3i}^2 \\ p_{1i}^3 & p_{2i}^3 & p_{3i}^3 \end{bmatrix}}^{A_i} \overbrace{\begin{bmatrix} C(k) \\ C(k-1) \\ C(k-2) \end{bmatrix}}^{x} + \overbrace{\begin{bmatrix} p_{4i}^1 & p_{5i}^1 & p_{6i}^1 \\ p_{4i}^2 & p_{5i}^2 & p_{6i}^2 \\ p_{4i}^3 & p_{5i}^3 & p_{6i}^3 \end{bmatrix}}^{B_i} \overbrace{\begin{bmatrix} C_i(k) \\ T_i(k) \\ T_{ci}(k) \end{bmatrix}}^{u} + \overbrace{\begin{bmatrix} h_i^1 \\ h_i^2 \\ h_i^3 \end{bmatrix}}^{h_i} \right), \tag{6}$$

where the superscript $\iota = 1, 2, 3$ indicates the number for each learned state. The polytopic equation is rewritten as a state-space presentation:

$$x(k+1) = \sum_{i=1}^{N_v} \bar{\mu}_i(\theta(k))\Big(A_i x(k) + B_i u(k) + h_i\Big),$$
$$y(k) = Cx(k), \tag{7}$$

In this context, $A_i \in \mathbb{R}^{n_x \times n_x}$, $B_i \in \mathbb{R}^{n_x \times n_u}$, $h_i \in \mathbb{R}^{n_x}$, and $C \in \mathbb{R}^{n_y \times n_x}$ denote the system matrices, and $y(k) \in \mathbb{R}^{n_y}$ is calculated based on these matrices. It is essential to note that the system is subject to uncertainties originating from model mismatches model, such that Takagi-Sugeno is structured as follows:

$$x(k+1) = \sum_{i=1}^{N_v} \bar{\mu}_i(\theta(k))\Big((A_i + \Delta A_i)x(k) + B_i u(k) + h_i\Big),$$
$$y(k) = Cx(k), \tag{8}$$

Here, ΔA_i represents the level of uncertainty. The uncertain matrices' magnitudes are directly linked to the fuzzy parameter values, and they are fine-tuned based on the minimum deviation to encapsulate the nominal values of the convex model. This adjustment process is carried out iteratively in the course of ANFIS learning. During this iterative learning, recursive least squares (RLS) play a key role in determining the optimal values for the covariance matrix, which encapsulates parameter uncertainties. The uncertainty in the TS model parameters is quantified using the error covariance matrix obtained from the fuzzy parameter estimation process. The covariance matrix for matrix A_i is expressed as:

$$\text{Cov}(A_i) = \begin{bmatrix} \sigma_{p_{11}}^2 & 0 & 0 \\ 0 & \sigma_{p_{22}}^2 & 0 \\ 0 & 0 & \sigma_{p_{33}}^2 \end{bmatrix}, \tag{9}$$

where $\sigma_{p_{ij}}^2$ indicates the variance of the parameter estimation for the ij-th element of matrix A_i. From equation (9), the uncertainty matrix ΔA_i is derived, representing the standard deviations of the fuzzy parameter estimates:

$$\varDelta A_i = \begin{bmatrix} \sigma_{p_{11}} & 0 & 0 \\ 0 & \sigma_{p_{22}} & 0 \\ 0 & 0 & \sigma_{p_{33}} \end{bmatrix}, \tag{10}$$

in this formulation, $\sigma_{p_{ij}}$ in equation (10) corresponds to the standard deviation for each fuzzy parameter of matrix A, indicating the inherent uncertainties within the model parameters and aiding in the assessment of the system's robustness and reliability. Additionally, it is presupposed that the uncertainties adhere to certain limits, outlined as follows:

$$\underline{\varDelta A_i} \leq \varDelta A_i \leq \overline{\varDelta A_i}. \tag{11}$$

The fault detection test relies on generating residuals to assess the consistency of measurements with system data. Nevertheless, parametric uncertainty prevents obtaining an exact estimate of the state $x(k)$ for direct data comparison. However, by taking into account (8), an observer is formulated to furnish an interval estimate of $x(k)$. This interval estimate encompasses both lower and upper bounds of $x(k)$, ensuring that:

$$\underline{\hat{x}}(k) \leq x(k) \leq \overline{\hat{x}}(k). \tag{12}$$

Given the uncertainty inherent in the system, the following fault diagnosis observer is put forth.

3.2. Design of the interval observer for fault detection

Interval observer-based fault detection is used to diagnose faults in dynamic systems, considering the presence of unknown but bounded uncertainty. This methodology is advantageous when precise information about the system parameters is unavailable, or the measurements have uncertainties or noise. An interval observer-based approach establishes an uncertain range for unknown or system parameters. This range is defined using intervals or sets of possible values instead of point values. Interval observers are designed to estimate both the system's current state and the associated uncertainty range.

The major advantage of interval observers is that they provide a method to deal with uncertainty without knowing its distribution. Instead of requiring an accurate and complete model system, these observers use the available data on the uncertain parameters' upper and lower limits or bounds. The interval observer is designed to propagate and contain the unknown but bounded uncertainty, allowing adaptive thresholds to be obtained for fault detection. This methodology improves the ability to detect faults under variable operating conditions and increases the system's robustness against uncertainties and external variations. Hence, estimates of the states of the system can be obtained, and any significant deviations from the expected values can be detected. By considering the unknown but fixed uncertainty, this technique allows early detection of anomalies or abnormal behaviors in the system, boosting decision-making and the corrective actions implementation.

Then, the following fault diagnosis observer is proposed by considering this uncertain system:

$$
\begin{aligned}
\underline{\hat{x}}(k+1) = \sum_{i=1}^{N_v} \bar{\mu}_i(\theta(k))\Big(& (A_i - \underline{L}_i C)\underline{\hat{x}}(k) + B_i u(k) + h_i + \underline{\Delta A_i}^{+}\underline{\hat{x}}^{+}(k) - \\
& \overline{\Delta A_i}^{+}\underline{\hat{x}}^{-}(k) - \underline{\Delta A_i}^{-}\underline{\hat{x}}^{+}(k) + \overline{\Delta A_i}^{-}\overline{\hat{x}}^{-}(k) + \underline{L}_i y(k)\Big), \\
\overline{\hat{x}}(k+1) = \sum_{i=1}^{N_v} \bar{\mu}_i(\theta(k))\Big(& (A_i - \overline{L}_i C)\overline{\hat{x}}(k) + B_i u(k) + h_i + \overline{\Delta A_i}^{+}\overline{\hat{x}}^{+}(k) - \\
& \underline{\Delta A_i}^{+}\overline{\hat{x}}^{-}(k) - \overline{\Delta A_i}^{-}\underline{\hat{x}}^{+}(k) + \underline{\Delta A_i}^{-}\underline{\hat{x}}^{-}(k) + \overline{L}_i y(k)\Big),
\end{aligned} \tag{13}
$$

where $\underline{L}_i$ and $\overline{L}_i$ are the observer gain matrices to be computed. $\overline{\Delta A_i}^{+} = \max\{0, \overline{\hat{x}}\}$, $\overline{\Delta A_i}^{-} = \overline{\Delta A_i}^{+} - \overline{\Delta A_i}$, $\underline{\Delta A_i}^{+} = \max\{0, \underline{\hat{x}}\}$, $\underline{\Delta A_i}^{-} = \underline{\Delta A_i}^{+} - \underline{\Delta A_i}$, $\overline{\hat{x}}^{+} = \max\{0, \overline{\hat{x}}\}$, $\overline{\hat{x}}^{-} = \overline{\hat{x}}^{+} - \overline{\hat{x}}$, $\underline{\hat{x}}^{+} = \max\{0, \underline{\hat{x}}\}$, $\underline{\hat{x}}^{-} = \underline{\hat{x}}^{+} - \underline{\hat{x}}$. The upper and lower values of the estimated output are obtained as:

$$\underline{y}(k) = C^{+}\hat{\underline{x}}(k) - C^{-}\hat{\overline{x}}(k) \tag{14}$$

$$\overline{y}(k) = C^{+}\hat{\overline{x}}(k) - C^{-}\hat{\underline{x}}(k) \tag{15}$$

where $C^{+} = \max\{0, C\}$ and $C^{-} = C^{+} - C$, subject to the observer equations given by (13). The main problem is to compute the gain matrices of the interval observer (13), such as the estimated states converge asymptotically to (14) and (15) despite the uncertainties. Under the assumption that:

$$\hat{\underline{x}}(0) \leq x(0) \leq \hat{\overline{x}}(0). \tag{16}$$

the dynamics of the errors of the interval $\underline{e}(k) = x(k) - \hat{\underline{x}}(k)$ and $\overline{e}(k) = \hat{\overline{x}}(k) - x(k)$, are defined as follows:

$$\begin{aligned} \underline{e}(k+1) = (A_i - \underline{L}_i C)\underline{e}(k) + \Delta A_i x(k) - \underline{\Delta A_i}^{+}\hat{\underline{x}}^{+}(k) + \\ \overline{\Delta A_i}^{+}\hat{\underline{x}}^{-}(k) + \underline{\Delta A_i}^{-}\hat{\underline{x}}^{+}(k) - \overline{\Delta A_i}^{-}\hat{\overline{x}}^{-}(k) \end{aligned} \tag{17}$$

$$\begin{aligned} \overline{e}(k+1) = (A_i - \overline{L}_i C)\overline{e}(k) - \Delta A_i(k) + \overline{\Delta A_i}^{+}\hat{\overline{x}}^{+}(k) - \\ \underline{\Delta A_i}^{+}\hat{\overline{x}}^{-}(k) - \overline{\Delta A_i}^{-}\hat{\underline{x}}^{+}(k) + \underline{\Delta A_i}^{-}\hat{\underline{x}}^{-}(k) \end{aligned} \tag{18}$$

The following sufficient conditions in the linear matrix inequalities (LMI) formulation are considered to solve this problem:

Theorem 3.1. *[30] Given an LMI region defined as:*

$$\mathscr{D} = \{z \in : f_{\mathscr{D}}(z) < 0\}, \tag{19}$$

where the characteristic function $f_{\mathscr{D}(z)}$ is defined as:

$$f_{\mathscr{D}(z)} = \alpha + z\varphi + z^{*}\varphi^{T} = \{\alpha_{kl} + \varphi_{kl}z + \varphi_{lk}z^{*}\}_{k,l\in[1,m]}, \tag{20}$$

with $\alpha = \alpha^{T} \in \mathbb{R}^{m\times m}$ and $\varphi \in \mathbb{R}^{m\times m}$, if there exist a diagonal matrix $P \in \mathbb{R}^{2n_x\times 2n_x}$, a symmetric matrix $Q = Q^{T} \in \mathbb{R}^{2n_x\times 2n_x}$, block diagonal matrices $W_i \in \mathbb{R}^{2n_x\times 2n_x}, i = 1, 2, \ldots, N$, with the following structure:

$$W_i = \begin{pmatrix} \underline{W_i} \in \mathbb{R}^{n_x\times n_x} & 0 \\ 0 & \overline{W_i} \in \mathbb{R}^{n_x\times n_x} \end{pmatrix} \tag{21}$$

and constants $\varepsilon_1 > 0$, $\varepsilon_2 > 0$, $\gamma > 0$ such that:

$$P > 0 \tag{22}$$

$$Q > 0 \tag{23}$$

and, for i=1,2,...,N:

$$\begin{pmatrix} \frac{P}{1+\varepsilon_1} & PD_i - W_i\gamma & \frac{P}{1+\varepsilon_1} \\ (PD_i - W_i\gamma)^T & P - Q - \gamma\eta^2 I_{2n_x} & 0 \\ \frac{P}{1+\varepsilon_1} & 0 & \gamma I_{2n_x} - \varepsilon P \end{pmatrix} \geq 0 \tag{24}$$

$$P \begin{bmatrix} A_i & 0 \\ 0 & A_i \end{bmatrix} - W_i\gamma \geq 0 \tag{25}$$

$$\left\{ \begin{array}{l} \alpha_{kl} P + \varphi_{kl} \left(\begin{pmatrix} A_i^T & 0 \\ 0 & A_i^T \end{pmatrix} P - \gamma^T W_i^T \right) \\ + \varphi_{kl} \left(P \begin{pmatrix} A_i & 0 \\ 0 & A_i \end{pmatrix} - W_i\gamma \right)_{k,l\in[1,m]} \end{array} \right. < 0 \tag{26}$$

with:

$$D_i = \begin{pmatrix} A_i + \underline{\Delta A_i}^+ & 0 \\ 0 & A_i + \overline{\Delta A_i}^+ \end{pmatrix} \tag{27}$$

$$\gamma = \begin{pmatrix} C & 0 \\ 0 & C \end{pmatrix} \tag{28}$$

$$\eta = 2 \max_{i=1,\ldots,N} \left(\|\underline{\Delta A_i}^+ - \overline{\Delta A_i}^+\|_2 + \|\underline{\Delta A_i}^-\|_2 + \|\overline{\Delta A_i}^-\|_2 \right) \tag{29}$$

$$\varepsilon = 1 + \varepsilon_2 + (1 + \varepsilon_1)^{-1} \tag{30}$$

then, the TS interval observer (13) with gains calculated as:

$$\underline{L}_i = P^{-1}\underline{W}_i \tag{31}$$

$$\overline{L}_i = P^{-1}\overline{W}_i \tag{32}$$

ensure the estimation of the interval $x(k)$ given by (12), provided that (13) and (16) are fulfilled.

Proof. The proof of the theorem can be consulted in Appendix A. ∎

The overall system of LMIs (22),(23),(24),(25) and (26) can be solved with software, for example, SeDuMi or Mosek can be used together with the Yalmip toolbox.

3.3. Residual generation scheme

By considering the estimated outputs (14–15), the following residuals can be obtained as:

$$\underline{r}(k) = y(k) - \overline{y}(k); \tag{33}$$

$$\overline{r}(k) = y(k) - \underline{y}(k); \tag{34}$$

where $r(k) \in \mathbb{R}^{N_y}$ is the residual. In the ideal case, $r(k) \approx 0$ if no faults are present. However, it may be non-zero in a fault-free scenario due to measurement noise and modeling errors.

Formulating the fault detection test involves establishing clear criteria based on the residual limits. If the calculated residual for a system output is outside the defined interval, the presence of a system fault can be inferred. This approach not only provides early detection of faults but also allows a quantitative evaluation of the severity of the fault since the magnitude of the residue indicates the deviation of the system from its normal behavior.

The passive approach is characterized by its ability to detect faults without an additional excitation signal. Rather, it is based on continuously monitoring system outputs and analyzing generated residuals. The adaptive threshold plays an essential role in this approach since it allows the dynamic adjustment of the acceptability limits of the residue based on the system parameters' uncertainties. A passive and robust approach based on an adaptive threshold [31] can improve fault detection. This approach can limit system parameter uncertainties' impact on the residual $r(k)$ associated with each output $y(k)$. In the absence of fault, said residual should include the zero value within a predefined interval.

$$y(k) \in \left[\underline{y}(k), \overline{y}(k)\right] \tag{35}$$

where $y(k)$ is the output, and $\underline{y}(k)$ and $\overline{y}(k)$ are the limits of the predicted output given by (14) and (15).

The formation of residuals is based on the estimated variables outlined in Table 3, and dedicated observers will be devised specifically for monitoring these dynamic residuals:

$$r_1(k) = C(k) - \hat{C}(k), \tag{36}$$

$$r_2(k) = T(k) - \hat{T}(k), \tag{37}$$

$$r_3(k) = T_c(k) - \hat{T}_c(k), \tag{38}$$

$$r_4(k) = Q_c(k) - \hat{Q}_c(k), \tag{39}$$

$$\tag{40}$$

In a fault case, the residuals are activated when exceeding the limits of the interval. If the interval limits are well defined, all false alarms can be avoided because the analytical relationships between sensors (inputs and outputs) guarantee the separability of the effect of each fault on the residuals. These residuals are stored in a fault incidence matrix, whose elements are constructed by considering the following logic:

$$\psi_{i,j}(k) = \begin{cases} 0 & \text{if} \quad r_i(k) \in \left[\underline{r_i}(k), \overline{r_i}(k)\right] \\ 1 & \text{if} \quad r_i(k) \notin \left[\underline{r_i}(k), \overline{r_i}(k)\right] \end{cases} , i = 1, 2, \ldots, N_y;\ j = 1, 2, \ldots, N_f. \tag{41}$$

where N_f is the number of faults. This matrix systematically records the activation of residuals for different fault scenarios, with columns representing specific faults and rows indicating individual residuals. Binary values within the matrix—"1" for activation and "0" for non-activation—map the response of the system's residuals to various faults. This structured approach enables fault isolation by comparing observed residual activation signatures against the predefined matrix, facilitating the identification of specific fault types. The fault incidence matrix is a tool in the diagnostic framework, ensuring fault detection and isolation based on distinct signatures of residual responses.

4. Results

This section presents the results of fault detection and isolation obtained in various scenarios described for the bioreactor system, as mentioned in Section 2. Table 2 summarizes all the evaluated faults. The configuration and data used in the numerical simulations are as follows:

- Nutrient flow profile, 100 L/h.
- Simulation time, 1200 min.
- Sampling rate, four samples per minute.
- Data vector for each variable, consisting of 4 800 samples.

For effective learning and to avoid overfitting of ANFIS, the datasets from each variable were divided into three subsets: 70% as the training subset, 15% as the testing subset, and 15% as the validation subset.

Table 5 contains the training results for the system identification, the number of fuzzy rules corresponding to the scheduling parameters obtained during ANFIS learning, and the Root Mean Square Error (RMSE) used to measure the accuracy of ANFIS obtained from the following equation:

$$\text{RMSE} = \sqrt{\frac{1}{N_\epsilon}\sum_{\epsilon=1}^{N_\epsilon}(y_\epsilon - \hat{y}_\epsilon)^2} \tag{42}$$

where y_ϵ is the target variable, $\hat{y}_\epsilon$ is the ANFIS output and N_ϵ is the number of data samples. Note that input perturbations change the dynamics of the system, such that measurements are distributed and correlated in a non-Gaussian manner. To train the ANFIS, 40 simulations were made in fault-free conditions. The difference between the simulations lies in the inputs with random seeds and process noise. The concentration variable (C_i) is centered around a mean of 1, and a random number generator block with a variance of 0.002 and seed generated by "randi(100000)" is added. For the temperature variables (T_i and T_{ci}), with a baseline of 350 Kelvin and a random number generator block with a variance of 2 and seed generated by "randi(100000)" is added. These specified ranges ensure that the simulations reflect the operating input spectrum, considering various conditions that could affect system performance. Figure 4 shows an example of the inputs.

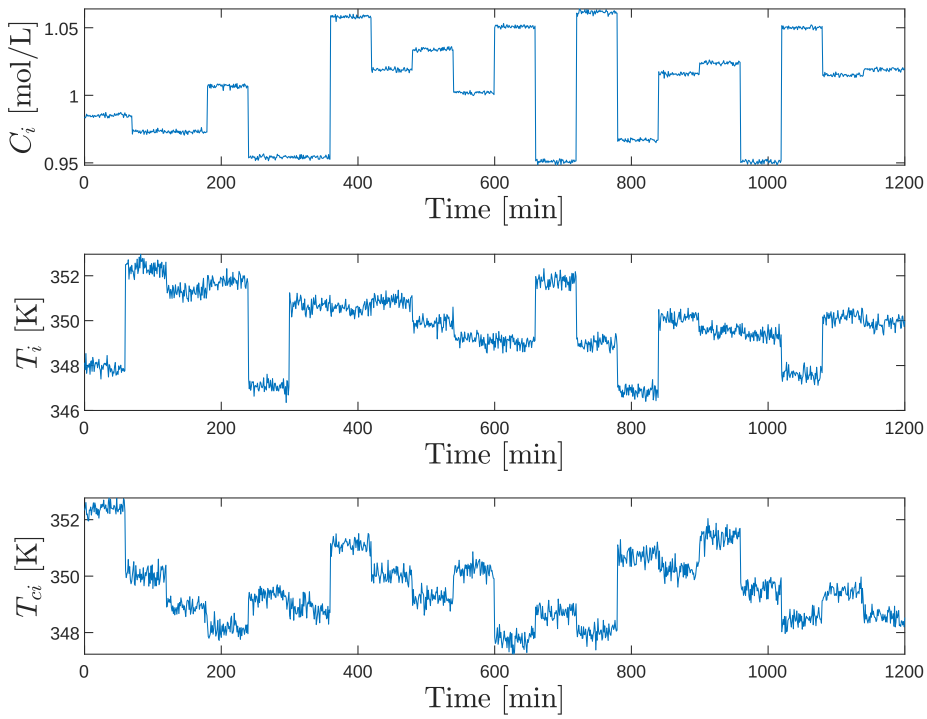

Figure 4: Random system inputs for CSTR simulation testing.

Table 4 summarizes the hyperparameters used in training for the ANFIS model in this study. The chosen hyperparameters, including the fuzzy structure, number of inputs and output, fuzzy rules, and specific settings for the training process, are optimized to enhance the model's predictive accuracy and computational efficiency.

Table 4: Hyperparameters of the ANFIS Model

Hyperparameter	Value
Fuzzy Structure	Takagi-Sugeno
Inputs/Output	6/1
Number of Fuzzy Rules	64
Membership Function Type	Generalized Bell-Shaped
Minimum Improvement	1×10^{-4}
Number of Epochs	150
Initial Step Size	0.01
Step Size Decrease Rate	0.8
Step Size Increase Rate	1.1

ANFIS training was carried out for each estimated variable in Table 3. The identification results of the nonlinear system of the bioreactor are presented in Table 5, the error metrics are averaged across all scenarios.

Table 5: Training results of each output variable of CSTR.

Related variable	Number of scheduling parameters	RMSE
$\hat{C}(k)$	64	7.1681x10^{-4}
$\hat{T}(k)$	64	4.8035x10^{-4}
$\hat{T}_c(k)$	64	4.9434x10^{-4}
$\hat{Q}_c(k)$	64	6.5689x10^{-4}

The process presented in Sections 3 is executed. Various simulations are done within the bioreactor system to yield a fault-free dataset and structure the polytopic TS systems. For instance, Figure 5 shows the plot of the interval observer corresponding to the concentration of the output product C; and Figure 6 shows the plot of the interval observer corresponding to the coolant flow-rate Q_c. The blue and yellow lines represent the upper and lower limits, respectively. These boundaries stand generated by the interval observer covering the C and Q_c variable in fault-free states. When a fault appears, and if it overextends these thresholds, it is a candidate to be considered according to the FDI method. The interval observers were designed appropriately, where the limits of the intervals are well defined, as seen in Figures 5 and 6. Consequently, all false positives can be avoided because the analytical relationships between the sensors guarantee the separability of the effect of each fault on the residuals contained in the fault signal matrix.

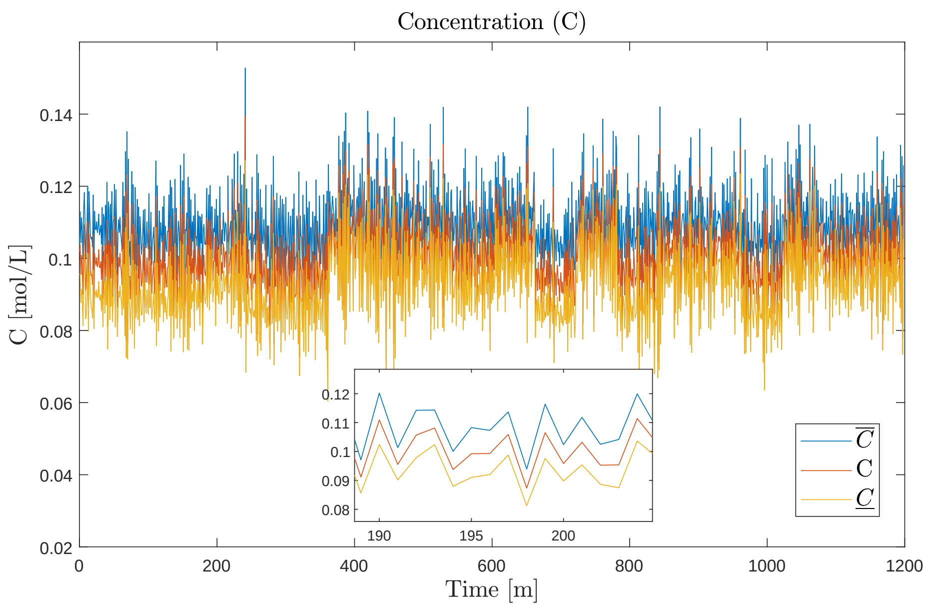

Figure 5: Interval observer of concentration of the output product.

A series of simulations were conducted to validate the proposed fault detection methodology. These simulations were based on the fault scenarios in Table 2 of Section 2 to assess the effectiveness of the interval observers implemented within the system. These observers demonstrated a high proficiency in detecting incipient faults, underscoring the robustness of this approach.

Specific instances are highlighted to understand the fault impacts and the observers' responses. Figure 7 clearly depicts Fault 1 of Catalyst decay affecting the concentration product. This incipient fault becomes detectable when it surpasses the lower threshold set by the observer, showcasing the sensitiv-

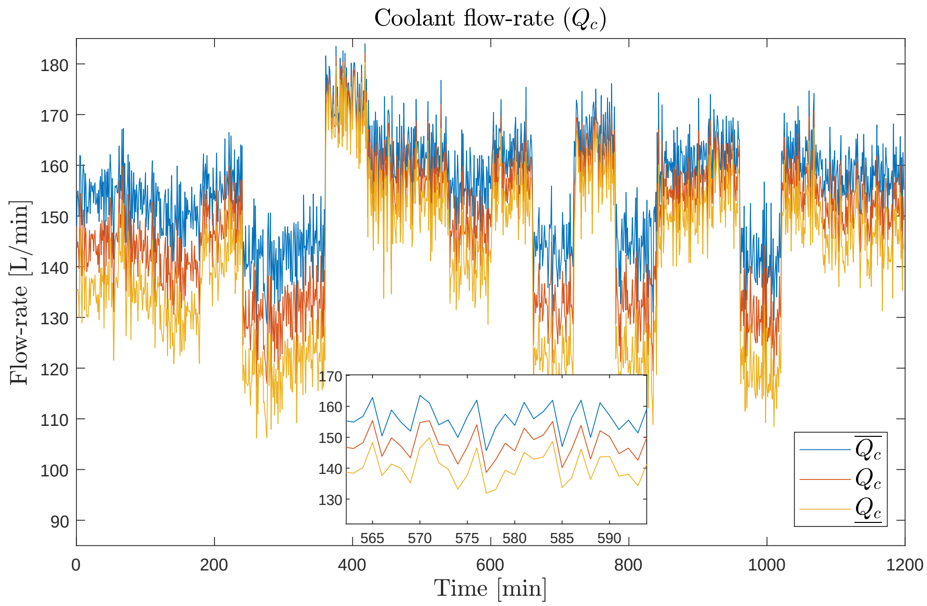

Figure 6: Interval observer of coolant flow-rate.

ity of our system to deviations from normal operating parameters. Similarly, Figure 8 offers an insightful visualization, where Fault 5, categorized as an incipient type, exceeds the upper threshold after 200 minutes of operation. This delayed response indicates the subtle nature of such faults and the necessity for sophisticated detection mechanisms like the one that has developed.

Beyond these individual cases, all other fault scenarios outlined were subjected to evaluation. The results of these assessments were systematically recorded in a fault incidence matrix, shown in Table 6. This matrix analyzes the patterns of each fault occurrence within the system. Although, in some cases, the same residuals are activated for the faults, it can be analyzed by columns and verify that a pattern exists for each fault case.

In the analysis of fault diagnosis within the CSTR system, two primary fault types are considered: multiplicative and additive. Faults categorized as multiplicative, specifically faults 1 to 3, are detected within 2 T_s or 30 seconds, considering a sampling time (T_s) of 15 seconds. These faults are indicative of progressive changes in process parameters. In contrast, additive faults, num-

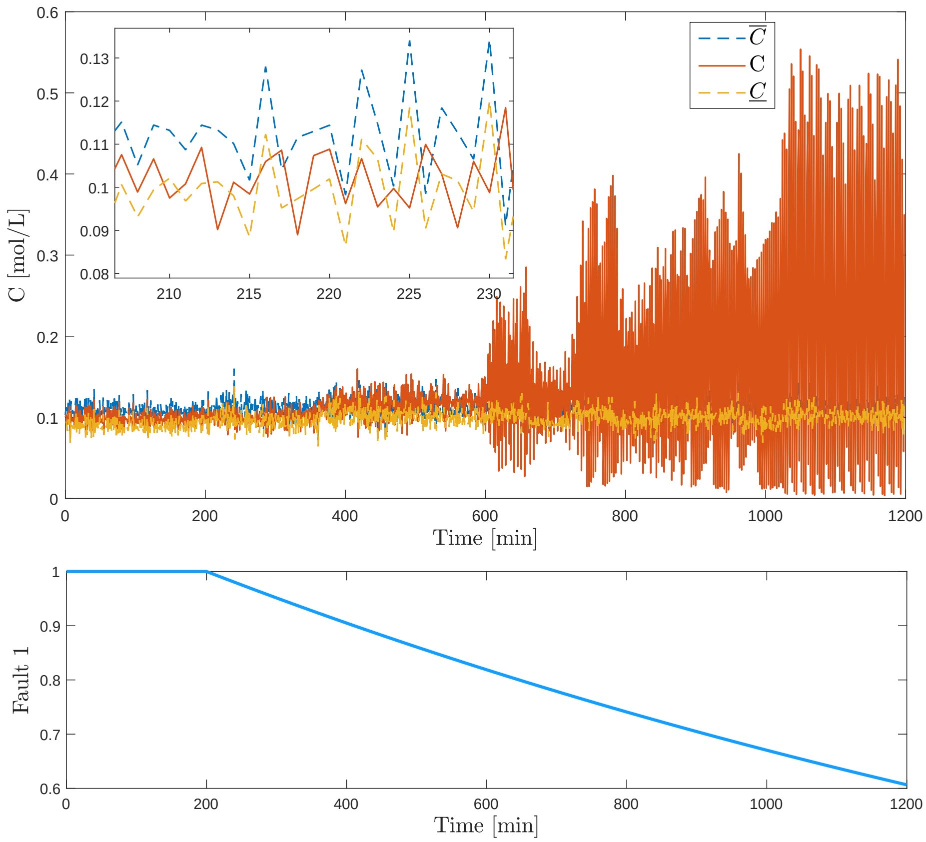

Figure 7: The concentration of the product affected by fault 1 of Catalyst decay.

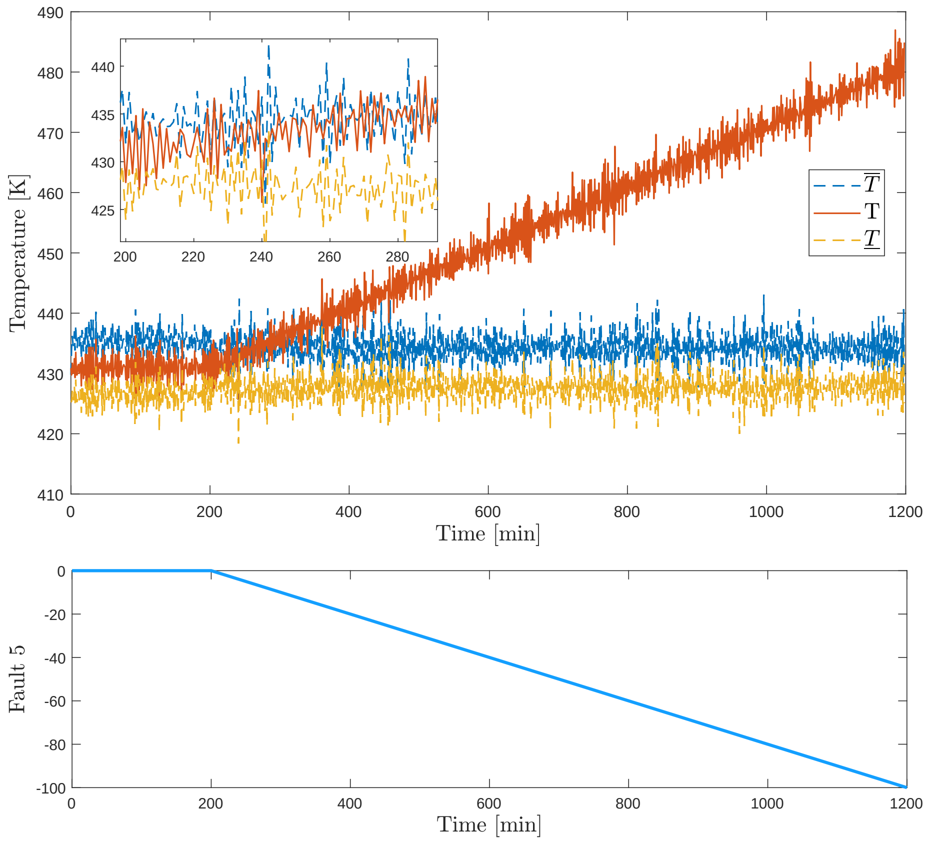

Figure 8: Fault 5 due to a bias in the T sensor.

Table 6: Fault signal matrix for seven of fault scenarios

FSM	f_1	f_2	f_3	f_4	f_5	f_6	f_7
r_1	1	0	1	1	0	0	0
r_2	0	1	1	0	1	0	0
r_3	1	0	1	0	0	1	0
r_4	0	1	1	0	0	0	1

bered 4 to 7, are identified within 3 T_s or 45 seconds. Such faults typically indicate immediate, linear deviations in system parameters or readings.

Further enhancing this analysis, the percentage change at the time of detection for each fault has been quantified to provide insight into the extent of the system's deviation from normal operating conditions. Table 7 illustrates the detection times for each fault within the system, along with the calculated percentage change, offering a comprehensive view of the fault impact and detection dynamics.

Table 7: Detection Times for Faults in CSTR with Percentage Change

Fault ID	Type	Time of Detection (T_s)	Percentage Change
1	Multiplicative	2	-0.025%
2	Multiplicative	2	-0.050%
3	Multiplicative	2	-0.075%
4	Additive	3	0.075%
5	Additive	3	0.011%
6	Additive	3	0.011%
7	Additive	3	-0.050%

5. Conclusions

This study has successfully demonstrated the ANFIS methodology's efficacy in modeling bioreactors' nonlinear dynamics. The training with ANFIS captured the complexities inherent in these systems and was also reflected in the precise prediction of output product concentrations. This highlights ANFIS's ability to represent bioreactor behavior accurately.

The convex Takagi-Sugeno systems derived from ANFIS proved efficient tools for designing interval observers in fault detection. These observers showcased remarkable robustness against uncertainties and measurement noise, common challenges in real-world industrial applications. The successful detection and isolation of all proposed fault cases using a fault incidence matrix further emphasize the system's ability to identify specific issues within the bioreactor process.

Compared to other machine learning approaches, a notable advantage of this method is its reliance solely on fault-free data. This aspect simplifies data collection and enhances the system's adaptability to varying operational conditions, a significant benefit for practical applications. Furthermore, this approach does not require knowledge of the system's dynamic equations. This independence from detailed mathematical models is a considerable advantage over other methods that depend on such information, making the proposed method more versatile and easier to implement in diverse bioprocess scenarios.

Lastly, the practical applicability of this method in industrial settings and types of bioreactors makes it a valuable solution for a wide range of applications in biotechnology. Dynamic system identification under uncertainty and noise makes fault detection methods robust, and ANFIS does not require fault data or detailed knowledge of the system's dynamic equations.

This study focuses on applying ANFIS Type 3 with Takagi-Sugeno models, chosen for their compatibility with the interval observer design. Due to the potential of ANFIS type 2 to model fuzzy intervals, future exploration is considered for the identification stage. Future work will address the integration of this methodology with other predictive maintenance strategies.

However, there are some limitations of the current study. Although the method has shown promising results in simulations, realistic applications can present additional challenges, such as more complex noise patterns and unexpected fault types. These factors can significantly distort the fault signals, affecting the effectiveness of the method. Overcoming these challenges requires functional knowledge of the system through available sensor data. Future work will focus on integrating this methodology with other predictive maintenance strategies. This integration aims to improve detection effectiveness and continuous adaptation to new fault conditions, ensuring a dynamic and up-to-date diagnostic response. Further research is expected to validate these strategies under real operating conditions to confirm their feasibility and robustness, thereby expanding the applicability of the method in complex industrial scenarios.

Acknowledgment

Tecnológico Nacional de México has supported this research under the program *Proyectos de Investigación Científica, Desarrollo Tecnológico e Innovación 2023*, project number 18984.23-P.

Appendix A. Proof of Theorem 3.1

Based on the analysis of [30], and considering the dynamics of the interval errors (17), if (25) is fulfilled, then:

$$A_i - \underline{L}_i C,\ A_i - \overline{L}_i \in \mathbb{R}_+^{n\times n} \tag{A.1}$$

where $\mathbb{R}_+^{n\times n}$ denotes the set of real matrices with nonnegative elements. Therefore, the dynamics of (17) is cooperative [32], and $x(k)$ is maintained while the uncertainties are limited, and its elements are positive, following (11).

To demonstrate that $\underline{\hat{x}}$ and $\overline{\hat{x}}$ remain bounded for all $k \geq 0$, the equations in (13) are rewritten as:

$$\underline{\hat{x}}(k+1) = [A_i - \underline{L}_i C + \underline{\Delta A_i}^+]\underline{\hat{x}}(k) + \underline{w_i}(\underline{\hat{x}}(k), \overline{\hat{x}}(k)) + \underline{\delta}_i(k) \tag{A.2}$$

$$\overline{\hat{x}}(k+1) = [A_i - \overline{L}_i C + \overline{\Delta A_i}^+]\overline{\hat{x}}(k) + \overline{w_i}(\underline{\hat{x}}(k), \overline{\hat{x}}(k)) + \overline{\delta}_i(k) \tag{A.3}$$

With:

$$\underline{w_i}(\underline{\hat{x}}(k), \overline{\hat{x}}(k)) = (\underline{\Delta A_i}^+ - \overline{\Delta A_i}^+)\underline{\hat{x}}^-(k) - \underline{\Delta A_i}^- \underline{\hat{x}}^+(k) + \overline{\Delta A_i}^- \overline{\hat{x}}^-(k) \tag{A.4}$$

$$\overline{w_i}(\underline{\hat{x}}(k), \overline{\hat{x}}(k)) = (\overline{\Delta A_i}^+ - \underline{\Delta A_i}^+)\overline{\hat{x}}^-(k) - \overline{\Delta A_i}^- \underline{\hat{x}}^+(k) + \underline{\Delta A_i}^- \overline{\hat{x}}^-(k) \tag{A.5}$$

$$\underline{\delta}_i(k) = \underline{L}_i y(k) - |\underline{L}_i| \tag{A.6}$$

$$\overline{\delta}_i(k) = \overline{L}_i y(k) - \left|\overline{L}_i\right| \tag{A.7}$$

Then, the boundedness of $\underline{\hat{x}}$ and $\overline{\hat{x}}$ is a consequence of the nonnegativity of $A_i - \underline{L}_i C + \underline{\Delta A_i}^+$ and $A_i - \overline{L}_i C + \overline{\Delta A_i}^+$, the boundedness of the inputs $\underline{\delta}_i(k)$ and $\overline{\delta}_i(k)$ and the property of the functions $\underline{w_i}$ and $\overline{w_i}$ of being globally Lipschitz [30], and is proved by introducing the system:

$$\xi(k+1) = G_i \xi(k) + \phi_i(\xi(k)) + \delta_i \tag{A.8}$$

where

$$\xi(k) = \begin{pmatrix} \underline{\hat{x}}(k) \\ \overline{\hat{x}}(k) \end{pmatrix} \phi_i(\xi(k)) = \begin{pmatrix} \underline{w}_i(\xi(k)) \\ \overline{w}_i(\xi(k)) \end{pmatrix} \delta_i(k) = \begin{pmatrix} \underline{\delta}_i(k) \\ \overline{\delta}_i(k) \end{pmatrix} \tag{A.9}$$

$$G_i = D_i - \begin{pmatrix} \underline{L}_i & 0 \\ 0 & \overline{L}_i \end{pmatrix} \Lambda \tag{A.10}$$

And:

$$|\phi_i(\xi(k))| \leq \eta \, |\xi(k)| \tag{A.11}$$

with η defined as in (30). In fact, using Schur complement, it can be shown that if (24) holds, the following is true for the increment $\Delta V(k)$ of the Lyapunov function $V(k) + \eta(k)^T P \eta(k)$ [30]:

$$\Delta V(k) \geq -\eta(k)^T Q\eta(k) + (1+\varepsilon_1^{-1}+\varepsilon_2^{-1})\delta_i(k)^T P\delta_1(k) \tag{A.12}$$

that proves the boundedness of $\underline{\hat{x}}$ and $\overline{\hat{x}}$.

Ultimately, it is essential to demonstrate that the closed-loop poles of the interval observer TS reside within the set $\mathscr{D}$, as defined in [33]. This task can be approached with relative simplicity, as the closed-loop matrix of the interval observer TS is expressed as follows:

$$A_{cl,i} = \begin{pmatrix} A_i & 0 \\ 0 & A_i \end{pmatrix} - \begin{pmatrix} \underline{L}_i & 0 \\ 0 & \overline{L}_i \end{pmatrix} \Lambda \tag{A.13}$$

In this manner, [30] is derived through the direct application of Theorem 2.2 in [34] to the matrix $A_{cl,i}$. This step concludes the proof.

References

[1] K. Bilodeau, D. Mantovani, Bioreactors for tissue engineering: focus on mechanical constraints. a comparative review, Tissue engineering 12 (2006) 2367–2383.

[2] F. Garcia-Ochoa, E. Gomez, Bioreactor scale-up and oxygen transfer rate in microbial processes: an overview, Biotechnology advances 27 (2009) 153–176.

[3] C. Ündey, S. Ertunç, T. Mistretta, B. Looze, Applied advanced process analytics in biopharmaceutical manufacturing: Challenges and prospects in real-time monitoring and control, Journal of Process Control 20 (2010) 1009–1018.

[4] I. Torres, J. D. Avilés, Observer-based sensor fault detection in a dark fermenter for hydrogen production, IEEE Control Systems Letters 5 (2020) 1621–1626.

[5] N. Md Nor, C. R. Che Hassan, M. A. Hussain, A review of data-driven fault detection and diagnosis methods: Applications in chemical process systems, Reviews in Chemical Engineering 36 (2020) 513–553.

[6] S. Venkateswaran, Q. Liu, B. A. Wilhite, C. Kravaris, Design of linear residual generators for fault detection and isolation in nonlinear systems, International Journal of Control 95 (2022) 804–820.

[7] S. Mitra, G. S. Murthy, Bioreactor control systems in the biopharmaceutical industry: a critical perspective, Systems Microbiology and Biomanufacturing (2022) 1–22.

[8] U. Imtiaz, A. Assadzadeh, S. S. Jamuar, J. Sahu, Bioreactor temperature profile controller using inverse neural network (inn) for production of ethanol, Journal of Process Control 23 (2013) 731–742.

[9] P. P. Mondal, A. Galodha, V. K. Verma, V. Singh, P. L. Show, M. K. Awasthi, B. Lall, S. Anees, K. Pollmann, R. Jain, Review on machine learning-based bioprocess optimization, monitoring, and control systems, Bioresource technology (2022) 128523.

[10] F. Clementschitsch, K. Bayer, Improvement of bioprocess monitoring: development of novel concepts, Microbial cell factories 5 (2006) 1–11.

[11] S. X. Ding, Advanced methods for fault diagnosis and fault-tolerant control, Springer, 2021.

[12] N. Sawattanakit, V. Jaovisidha, Process fault detection and diagnosis in cstr system using on-line approximator, in: IEEE. APCCAS 1998. 1998 IEEE Asia-Pacific Conference on Circuits and Systems. Microelectronics and Integrating Systems. Proceedings (Cat. No. 98EX242), IEEE, 1998, pp. 747–750.

[13] D.-H. Zhou, P. Frank, Fault diagnostics and fault tolerant control, IEEE Transactions on aerospace and electronic systems 34 (1998) 420–427.

[14] A. P. Deshpande, S. C. Patwardhan, S. S. Narasimhan, Intelligent state estimation for fault tolerant nonlinear predictive control, Journal of Process control 19 (2009) 187–204.

[15] M. Gholizadeh, A. Yazdizadeh, H. Mohammad-Bagherpour, Fault detection and identification using combination of ekf and neuro-fuzzy network applied to a chemical process (cstr), Pattern Analysis and Applications 22 (2017) 359–373.

[16] V. K. Kannan, R. Srimathi, V. Gomathi, R. Valarmathi, L. PrithiEkammai, Investigation of unknown input observer for sensor fault diagnosis for a cstr process, Materials Today: Proceedings 45 (2021) 3431–3437.

[17] G. Ortiz-Torres, J. Rumbo-Morales, F. Sorcia-Vázquez, A. Pérez-Vidal, A. Cruz-Rojas, J. Brizuela-Mendoza, E. Oceguera-Contreras, Concentration estimation and fault tolerant control in a cstr modelled as a quasi linear parameter varying system, Revista Mexicana de Ingeniería Química 20 (2021) 51–66.

[18] P. Du, J. A. Venkidasalapathy, S. Venkateswaran, B. Wilhite, C. Kravaris, Model-based fault diagnosis and fault tolerant control for safety-critical chemical reactors: A case study of an exothermic continuous stirred-tank reactor, Industrial & Engineering Chemistry Research 62 (2023) 13554–13571.

[19] S. Venkateswaran, M. Z. Sheriff, B. Wilhite, C. Kravaris, Design of functional observers for fault detection and isolation in nonlinear systems in the presence of noises, Journal of Process Control 108 (2021) 68–85.

[20] J. D. Aviles, I. Torres-Zúñiga, A. Villa-Leyva, A. Vargas, G. Buitrón, Experimental validation of an interval observer-based sensor fault detection strategy applied to a biohydrogen production dark fermenter, Journal of Process Control 114 (2022) 131–142.

[21] H. Pan, X. Yu, Y. She, B. Teng, L. Li, J. Hu, Fault estimation and self-healing control of discrete-time ts fuzzy model with sensor and actuator faults based on dual observers, Journal of Process Control 130 (2023) 103070.

[22] H. Pan, X. Yu, J. Hu, L. Li, Y. She, Y. Zhang, H. Zan, A self-healing controller based on sliding-mode control for sensor fault in wastewater treatment processes, Journal of Process Control 127 (2023) 102997.

[23] A. Azarbani, A. Fakharian, M. B. Menhaj, On the design of an unknown input observer to fault detection, isolation, and estimation for uncertain multi-delay nonlinear systems, Journal of Process Control 128 (2023) 103018.

[24] U. S. Banu, G. Uma, Anfis based sensor fault detection for continuous stirred tank reactor, Applied Soft Computing 11 (2011) 2618–2624.

[25] H. Hosseini, M. Shahbazian, M. A. Takassi, The design of robust soft sensor using anfis network, Journal of Instrumentation Technology 2 (2014) 9–16.

[26] P. Jagtap, P. Raut, G. N. Pillai, F. Kazi, N. Singh, Extreme-anfis: A novel learning approach for inverse model control of nonlinear dynamical systems, in: 2015 International Conference on Industrial Instrumentation and Control (ICIC), IEEE, 2015, pp. 718–723.

[27] M. Mansouri, M. Nounou, H. Nounou, N. Karim, Kernel pca-based glrt for nonlinear fault detection of chemical processes, Journal of Loss Prevention in the Process Industries 40 (2016) 334–347.

[28] K. E. S. Pilario, Y. Cao, Canonical variate dissimilarity analysis for process incipient fault detection, IEEE Transactions on Industrial Informatics 14 (2018) 5308–5315.

[29] T. Takagi, M. Sugeno, Fuzzy identification of systems and its applications to modeling and control, IEEE transactions on systems, man, and cybernetics SMC-15 (1985) 116–132.

[30] D. Efimov, T. Raïssi, W. Perruquetti, A. Zolghadri, Estimation and control of discrete-time lpv systems using interval observers, in: 52nd IEEE Conference on Decision and Control, IEEE, 2013, pp. 5036–5041.

[31] V. Puig, J. Quevedo, T. Escobet, F. Nejjari, S. de las Heras, Passive robust fault detection of dynamic processes using interval models, IEEE Transactions on Control Systems Technology 16 (2008) 1083–1089.

[32] M. W. Hirsch, H. Smith, Monotone maps: a review, Journal of Difference Equations and Applications 11 (2005) 379–398.

[33] S. De Lira, V. Puig, J. Quevedo, A. Husar, Lpv observer design for pem fuel cell system: Application to fault detection, Journal of Power Sources 196 (2011) 4298–4305.

[34] M. Chilali, P. Gahinet, H/sub/spl infin//design with pole placement constraints: an lmi approach, IEEE Transactions on automatic control 41 (1996) 358–367.